Journal of Materials Chemistry A

Check for updates

A CoHCF system with enhanced energy conversion efficiency for low-grade heat harvesting†

Jing Jiang,‡[a] Hanqing Tian, [iD] ‡[a] Xinrui He,‡[a] Qing Zeng,[a] Yi Niu,[a] Ting Zhou,[a] Yuan Yang [iD] *[b] and Chao Wang [iD] *[a]

Thermally regenerative electrochemical cycles (TRECs) have drawn plenty of attention recently as an efficient and low-cost approach to convert heat to electricity. In this work, we report the application of cobalt hexacyanoferrate (CoHCF)-based materials in TRECs. When the battery is charged at a high temperature (T_H) and discharged at a low temperature (T_L), the discharge voltage is higher than the charge voltage due to the dependence of battery voltage on temperature, and thus low-grade heat can be converted into electricity. The temperature coefficient and specific heat of the material determine the energy conversion efficiency of the battery. When complexed with helical carbon nanotubes (HCNTs), the CoHCF/HCNTs show a higher absolute temperature coefficient and lower specific heat than pure CoHCF. Consequently, the heat-to-electricity conversion efficiency is greatly increased. It is suggested that moderately changing the temperature coefficient and specific heat is an effective strategy to further improve thermogalvanic performance of CoHCF-based materials.

1. Introduction

Low-grade waste heat (<100 °C) widely exists in the natural environment and industrial production processes.[1–4] It has great potential as a sustainable energy source due to its large quantity and wide distribution. However, efficient utilization of low-grade waste heat is challenging, since the theoretical efficiency is limited by the Carnot limit. Currently available technologies include solid-state thermoelectric energy conversion[5] and the organic Rankine cycle. Solid-state thermoelectric conversion needs materials with low abundance and high cost, and the organic Rankine cycle has complicated system designs.[5–8] In contrast, thermally regenerative electrochemical cycles (TRECs) can achieve relatively high heat-to-electricity conversion efficiency with low costs and facile assembly processes, which is attractive for low-grade heat harvesting.[9–13]

TRECs are based on the temperature-dependence of cell voltage in an electrochemical system. For a battery reaction, A + B → C + D, the temperature coefficient α is defined as:

$$\alpha = \frac{\partial V}{\partial T} = \frac{S_B}{nF} \tag{1}$$

where V is the full cell voltage, T is the temperature, n is the number of electrons transferred in the reaction,[14] F is Faraday's constant, and S_B stands for the change of partial molar entropy in the full cell reaction. In the case of α being negative, as shown in Fig. 1, the low-grade heat can be converted into electrical energy when the battery is charged at T_H and discharged at T_L, as the voltage at T_L is higher than that at T_H. In contrast, when α is positive, electrical energy is gained when the battery is charged at T_L and discharged at T_H. To evaluate the heat-to-electricity conversion efficiency, the conversion efficiency μ is defined as:

$$\mu = \frac{W}{Q_H + Q_{HR}} = \frac{S_B \Delta T - E_{loss}}{|\alpha| T_H Q_C + (1 - \mu_{HR}) \Delta T C_P} \tag{2}$$

where W is the energy difference between the battery charge and discharge in one cycle, Q_H stands for the energy absorbed at high temperatures, Q_{HR} stands for the extra energy which is used for heating the battery to complete the cycle, S_B is the change of partial molar entropy in the reaction, $\Delta T = T_H - T_L$, E_{loss} is the energy loss due to the internal resistance, C_p is the heat capacity of the battery and μ_{HR} is the energy recovery efficiency, indicating how much energy that dissipated during the cooling process can be used for the heating process. μ_{HR} can reach 100% theoretically and 50–70% practically.

Recently Prussian blue and its analogues were extensively investigated in TRECs.[15–17] Lee *et al.*[18] reported a TREC system with copper hexacyanoferrate as the cathode and Cu^{2+}/Cu as the anode, which achieved a high conversion efficiency of 5.7%

[a]*Clean Energy Materials and Engineering Center, School of Electronic Science and Engineering, State Key Laboratory of Electronic Thin Film and Integrated Devices, University of Electronic Science and Technology of China, Chengdu, Sichuan, China. E-mail: cwang@uestc.edu.cn*

[b]*Program of Materials Science and Engineering, Department of Applied Physics and Applied Mathematics, Columbia University, New York, New York 10025, USA. E-mail: yy2664@columbia.edu*

† Electronic supplementary information (ESI) available. See DOI: 10.1039/c9ta02426c
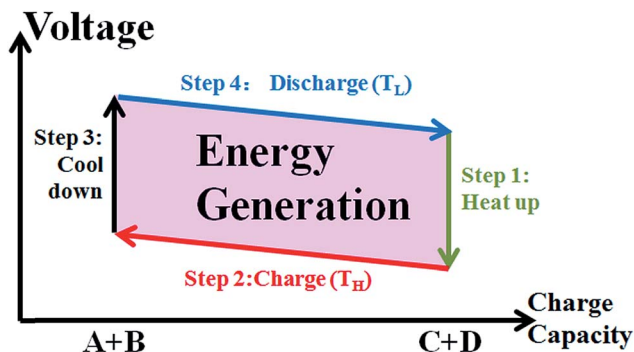
‡ These authors contributed equally to this work.

Fig. 1   The voltage–capacity plot of a TREC.

when charged at 60 °C and discharged at 10 °C. Yang *et al.*[9] reported a novel membrane-free battery where nickel hexacyanoferrate (NiHCF) and Ag^+/Ag served as the cathode and the anode, respectively, with a full cell temperature coefficient of -0.74 mV K^{-1}.

One challenge in these TREC systems is the reduction of cell impedance so that the voltage loss due to internal resistance is limited, and thus the heat-to-electricity conversion efficiency can be enhanced. Usually, complexing with carbon materials, such as carbon nanotubes, graphene and porous carbon, is an effective strategy by which the composites can form three-dimensional hybrid structures to realize facile Li^+ and electron transport, high conductivity and high surface area.[19–26]

In this work, we propose a novel approach of compositing with helical carbon nanotubes (HCNTs) to improve the heat-to-electricity conversion efficiency. Pure CoHCF shows an absolute temperature coefficient of 0.69 mV K^{-1} and a specific heat of 2.33 J g^{-1} K^{-1}. When complexed with HCNTs, the absolute temperature coefficient is improved to 0.89 mV K^{-1} and the specific heat capacity is reduced to 2.17 J g^{-1} K^{-1}. Consequently, the heat-to-electricity conversion efficiency of CoHCF/HCNTs is twice higher than that of pure CoHCF at different energy recovery efficiencies (μ_{HR}). It is suggested that moderate improvement of the absolute temperature coefficient and reduction of specific heat of materials indeed further improve the heat-to-electricity conversion performance of pure cobalt hexacyanoferrate materials.

2.   Experimental section

2.1   Synthesis and acid treatment of HCNTs

All chemicals used in the experiments were purchased from KESHI and were analytical reagent grade. Firstly, in a typical procedure, 100 mL of 1 mol $FeCl_2$ was added into 100 mL of a 1 mol $C_4H_4O_6KNa$ solution under constant stirring at room temperature. After the mixture turned light yellow, a precipitate was obtained by filtration. Then the precipitate was washed with deionized water several times until the pH of the solution became neutral. In order to remove residual organic impurities, the obtained product was washed in a Soxhlet extractor with ethanol for 3 h and dried in a vacuum oven at 90 °C for 3 h. Thus, the catalyst precursor $C_4H_4O_6Fe$ was obtained. The

HCNTs were prepared by a typical catalytic chemical vapor deposition (CCVD) method. $C_4H_4O_6Fe$ was used as the catalyst precursor and HCNTs were then synthesized in a horizontal reaction tube at 550 °C by introducing acetylene for 1 h. Details are shown in our previous work.[19] 1.2 g HCNTs were added into 400 mL mixed acid (300 mL H_2SO_4 (98%) and 100 mL HNO_3 (65%)), and then the mixture was sonicated for 100 min and diluted for the next process. After being centrifuged, the obtained precipitate was washed with deionized water several times until approximately neutral pH of the filtrate was obtained. Finally, after drying at 80 °C in a vacuum oven for 24 h, the functional HCNTs were obtained.

2.2   Synthesis of CoHCF and the CoHCF/HCNT nanocomposite

The CoHCF/HCNT composite was obtained by a chemical co-precipitation method. 0.2 g functional HCNTs were first added into 20 mL deionized water and then sonicated for 1 h and continuously stirred for 2 h. Then 20 mL of 25 mmol $K_3Fe(CN)_6$ (Sigma Aldrich) and 20 mL of 50 mmol $Co(NO_3)_2$ (Sigma Aldrich) were simultaneously added dropwise into the aqueous solution of HCNTs under strong stirring with a speed of about one drop per second. The black brown precipitate was centrifuged and dried at 40 °C for 12 h. The ratio of CoHCF to HCNTs is approximately equal to 3 : 4. For the sake of comparison, pure CoHCF was synthesized by the same chemical co-precipitation process without the addition of HCNTs.

2.3   Preparation of the electrode and electrochemical measurement

The electrochemical system was studied in a three-electrode configuration inside a pouch cell. The working electrode slurry was prepared by mixing 70 wt% as-prepared composite, 20 wt% super P carbon black and 10 wt% polyvinylidene fluoride (PVDF) in *N*-methyl-2-pyrrolidone (NMP) and then stirring for several hours. The obtained slurry was cast onto carbon cloth with an area of 1 cm × 1 cm and dried at 40 °C in a vacuum oven. The mass loading of the active material was about 2 mg cm^{-2}. Here, all chemicals used for preparation of the slurry were purchased from Power Battery Material Co. Ltd at battery grade quality. Pt and Ag foil pieces were used as current collectors for the working electrode and the counter electrode, respectively. The Ag/AgCl reference electrode was made by precharging a silver rod with a width of 2–5 mm in a 1 mol L^{-1} KCl solution at a current density of 1 mA cm^{-2} for 1 h. Then a Ag film with 15–20 mm width was charged in a 1 mol L^{-1} KCl solution at a current density of 1 mA cm^{-2} for 2 h and discharged for 0.7 h, resulting in the formation of a Ag/AgCl film for use as the counter electrode. A 3 mol L^{-1} KCl aqueous solution was used as the electrolyte.

2.4   Instruments

In the experiments, a centrifugal separator (TL80-1, Tianli, Jiangsu) was used to centrifuge the precipitate and an ultrasonic generator (KH2200E, Hechuang, Kunshan) was used for acid treatment of HCNTs. A vacuum oven (DZF-6020, Kejin, Hefei)

was used for drying the as-prepared composite and the electrode. Electrochemical properties were characterized using an electrochemical workstation (P4000, Princeton, USA). X-ray diffraction (XRD) patterns were obtained on an X-ray powder diffractometer (XRD-7000X) with Cu Kα radiation of wavelength $\lambda = 1.5418\,\text{Å}$, and a field emission scanning electron microscope (FESEM, JSM-7600F) was used to observe the morphology and size of composites. Specific heat (c_p) was measured using a Differential Scanning Calorimeter (DSC, Q2000 V24.7 Build 119). Temperature cycling was performed with a home-made thermoelectric-based temperature cycler, and will be described below.

3. Results and discussion

The morphologies of CoHCF, HCNTs and the CoHCF/HCNT composite are investigated by scanning electron microscopy (SEM) and the obtained results are presented in Fig. 2 and S1.† Fig. S1† shows homogeneous helical structures with an average coil diameter of 0.2 μm and coil pitch of 0.3 μm. Loops from different parts of the helical fiber come together and show similar size and morphology. Fig. 2a indicates that the average size of the CoHCF aggregations is about 3 μm, while the grain size is about 100 nm. As shown in Fig. 2b, CoHCF particles with sizes of 500–800 nm are uniformly dispersed around HCNTs, which form a continuous porous network. With the addition of HCNTs, the microtexture of CoHCF is improved and the CoHCF/HCNT composite shows better electrochemical performance than pure CoHCF.

X-ray diffraction (XRD) is used to further study the crystal structure of CoHCF and the CoHCF/HCNT composite. As shown in Fig. S2,† all diffraction peaks agree well with the standard diffraction pattern of $Co_3[Fe(CN)_6]_2 \cdot 2H_2O$ (ICSD, PDF file no. 82-2284) with no discernible impurity phase. The corresponding crystal planes are noted near the peaks. A broad characteristic diffraction peak of C (ICSD, PDF file no. 75-0444) centered at 26.31° can be obviously observed in the XRD pattern of the CoHCF/HCNT composite, which confirms the existence of HCNTs in the composite sample.

Electrochemical tests at room temperature are first investigated to study the intrinsic properties of the CoHCF and CoHCF/HCNTs. All electrochemical measurements are carried out with a three electrode configuration in a pouch cell, with
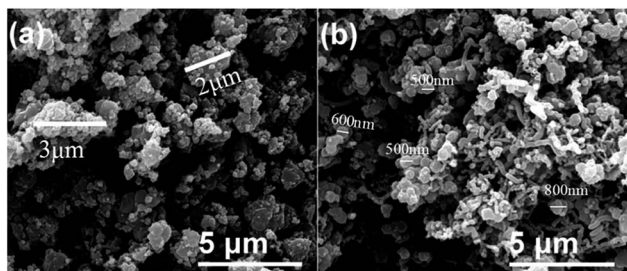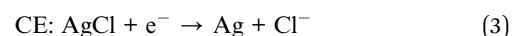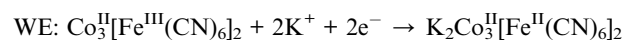
CoHCF or CoHCF/HCNTs as the working electrode (WE), and Ag/AgCl as both the reference and counter electrodes (Fig. S3†). The electrolyte is a 3 mol L^{-1} KCl aqueous solution and the typical amount of electrolyte inside the pouch cell is about 0.5 mL. The reactions of the two cells are:

$$\text{WE: } Co_3^{II}[Fe^{III}(CN)_6]_2 + 2K^+ + 2e^- \rightarrow K_2Co_3^{II}[Fe^{II}(CN)_6]_2$$

$$\text{CE: } AgCl + e^- \rightarrow Ag + Cl^- \tag{3}$$

The electrochemical performance including cyclic voltammetry (CV), galvanostatic charge/discharge (GCD), electrochemical impedance spectroscopy (EIS) and cycling stability of CoHCF and CoHCF/HCNT electrodes is evaluated at room temperature before temperature-dependent electrochemical property measurements. Fig. 3 shows that CoHCF and CoHCF/HCNTs possess good chemical reversibility. The cyclic voltammetry curves at different scanning speeds show similar shapes, and a pair of redox couples can be clearly identified (Fig. 3a and b), which reveals that the specific capacity of CoHCF mainly comes from ion intercalation/deintercalation of the electrode. Fig. 3c compares the cyclic voltammogram area of CoHCF and CoHCF/HCNTs. It is obvious that the CoHCF/HCNTs show a larger area than pure CoHCF at the same scanning speed of 5 mV s^{-1}, which demonstrates that the HCNT network enhances the kinetics of electrochemical reactions. After demonstrating steady performance at room temperature, the temperature-dependent electrochemical properties are investigated. The cell voltages of CoHCF and CoHCF/HCNTs at different temperatures are measured carefully as shown in Fig. 3d. Fig. 3d shows that the full battery voltage is linear with temperature in the range from T_L to T_H. Moreover, the CoHCF/HCNT composite exhibits lower equivalent series resistance and higher capacity than CoHCF as shown in Fig. S4.† The EIS curves tested at a sinusoidal signal of 10 mV in the frequency
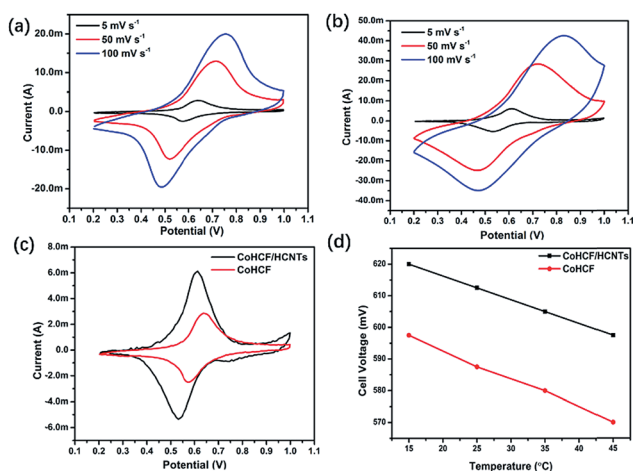

Fig. 2 SEM images of the as-prepared (a) CoHCF and (b) CoHCF/HCNT composite.

Fig. 3 (a) Cyclic voltammetry curves of CoHCF at different scan rates. (b) Cyclic voltammetry curves of CoHCF/HCNTs at different scan rates. (c) The comparison of cyclic voltammetry curves between CoHCF and CoHCF/HCNTs at 5 mV s^{-1}. (d) The temperature-dependent voltage of a pouch cell at different temperatures.

range of 100 kHz to 0.01 Hz are depicted. The impedance of the CoHCF/HCNT composite is lower than that of CoHCF. And the GCD is also analyzed from 520 to 680 mV. Apparently, the discharge time of CoHCF/HCNTs is also longer than that of

pure CoHCF. Moreover, Fig. S5† illustrates the cycling performance of this system. HCNTs are electrochemically unstable in aqueous media due to the supercapacitive properties, and after cycling for 1000 cycles, the final retention rate of HCNTs is reduced to approximately 50%. The CoHCF/HCNT system is charged and discharged for 10 cycles at a current density of 40 mA g^{-1}, and the specific capacity shows no obvious decrease. Therefore, compositing with HCNTs is an effective way to improve the electrochemical performance of CoHCF, which will be beneficial for its application in TREC systems.

Temperature-dependent electrochemical properties are measured with a homemade temperature cycler as shown in Fig. S6.† The thin pouch cell is sandwiched between two Al sheets, which are heated or cooled by thermoelectric plates. The thermal couples are attached to the surface of the cell for temperature measurement. The temperature is measured and controlled using an SCM (a temperature controller shown in Fig. S6b†). Fig. 4 and S7† show the temperature-dependent open-circuit voltage (OCV) of CoHCF, HCNTs and CoHCF/ HCNTs at different temperatures. The pure CoHCF and HCNTs show absolute temperature coefficients of 0.69 and 0.43 mV K^{-1}, respectively. When complexed with HCNTs, the absolute temperature coefficient is improved to 0.89 mV K^{-1}. The larger coefficient indicates the larger voltage gap between charge and discharge, which can enhance the heat-to-electricity
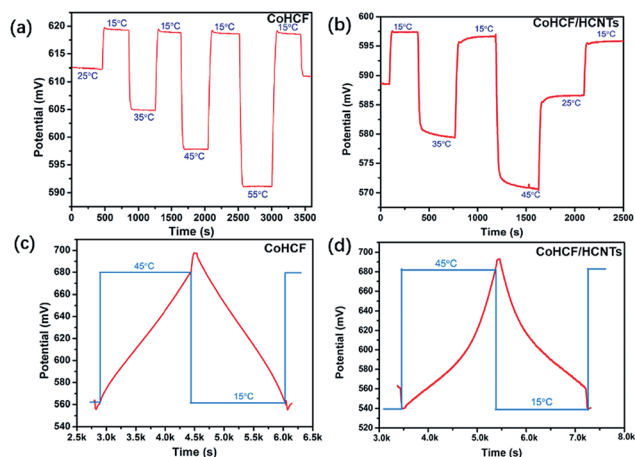

Fig. 4 The real time measurement of the temperature coefficient of (a) CoHCF and (b) the CoHCF/HCNT composite. The thermal cycling system at 40 mA g^{-1} for the (c) CoHCF/Ag/AgCl/3 M KCl electrochemical system and (d) CoHCF/HCNT/Ag/AgCl/3 M KCl electrochemical system.
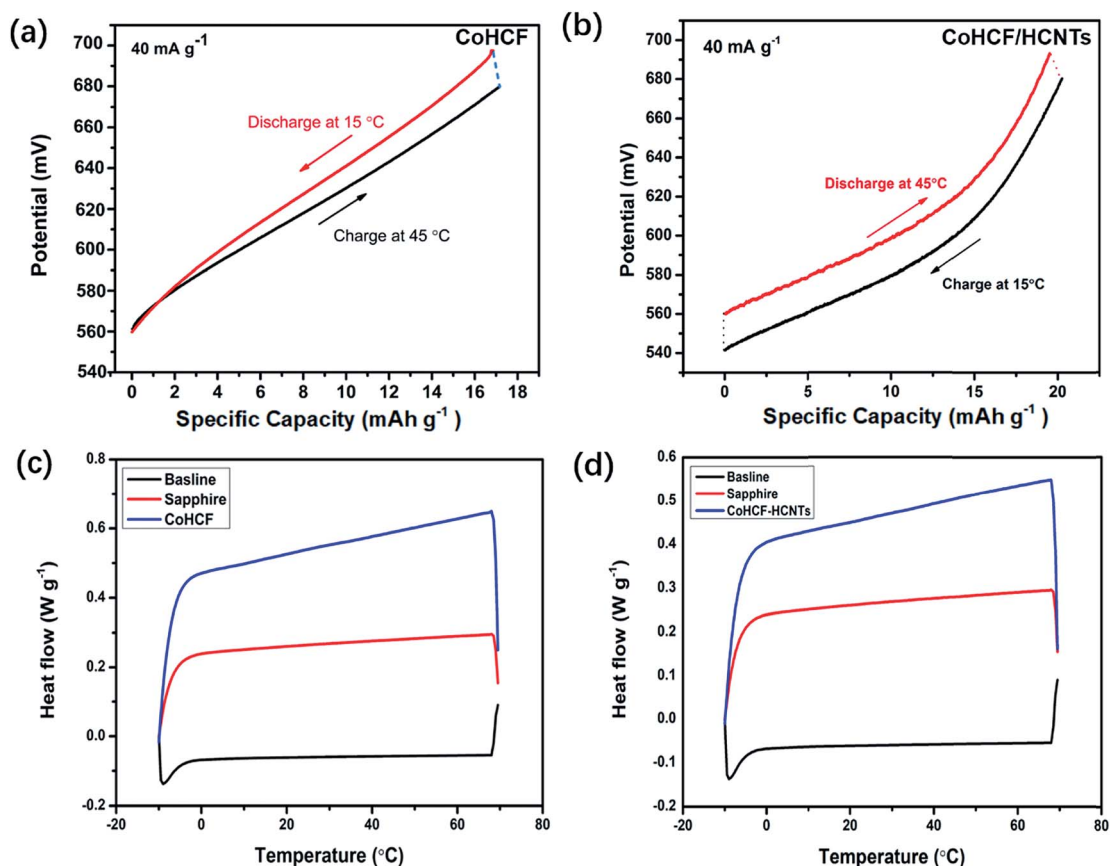

Fig. 5 The voltage *vs.* specific capacity plot at 40 mA g^{-1} of (a) CoHCF and (b) CoHCF/HCNTs, the heat flux as a function of the sample temperature in the DSC test of (c) CoHCF and (d) CoHCF/HCNTs.

conversion efficiency. The structure of the materials usually determines their properties. To further verify the increase of the absolute temperature coefficient, we recorded the SEM image of pure HCNTs first, which shows the homogeneous helical structures (Fig. S1†). Then, we obtained the BET and BJH results of the HCNTs. As shown in Fig. S8,† the specific area of HCNTs is 19.3 $m^2\ g^{-1}$ and the pore size distribution is mainly at 5–50 nm, indicating the presence of mesopores. Based on these data, we are able to hypothesize that the helical structures and large specific area may provide faster transport channels for ions and electrons, which results in a higher absolute temperature coefficient of CoHCF/HCNTs. Fig. 4c and d present the temperature cycles of CoHCF and CoHCF/HCNT electrodes, respectively. It can be obviously observed that the voltages increase when the temperature decreases from T_H to T_L. However, when the temperature increases from T_L to T_H, the voltage decreases at first and then increases.

The heat harvesting performance and specific heat of CoHCF, HCNT and CoHCF/HCNT electrodes are shown in Fig. 5 and S9.† The CoHCF and CoHCF/HCNT electrodes are charged/discharged at a constant current density of 40 mA g^{-1} as shown in Fig. 5a and b. For pure CoHCF, the pouch cell is charged to 697.60 mV at 45 °C, discharged at 15 °C to 555.40 mV, and then heated up to 45 °C again. The average discharge and charge voltages of CoHCF are 629.90 mV (V_{dis}) and 622.00 mV (V_{ch}), respectively. The charge capacity of CoHCF is 17.12 mA h g^{-1} (Q_{ch}) and discharge capacity is 16.87 mA h g^{-1} (Q_{dis}). Therefore, the gap between charge and discharge is only 7.9 mV, representing a small voltage gain. The small voltage gap and low efficiency of pure CoHCF originate from the low temperature coefficient and high impedance of the electrode. To address these issues, the CoHCF/HCNT composite is further tested between 15 °C and 45 °C, and the average discharge and charge voltages of CoHCF/HCNTs are 605.30 mV (V_{dis}) and 589.20 mV (V_{ch}), respectively. The charge capacity of CoHCF/HCNTs is 20.20 mA h g^{-1} (Q_{ch}) and discharge capacity is 19.50 mA h g^{-1} (Q_{dis}). The gap between charge and discharge is 16.1 mV, which is twice higher than that of pure CoHCF. The specific heat of HCNTs is 1.25 J g^{-1} K^{-1}, which is lower than that of pure CoHCF (2.33 J g^{-1} K^{-1}). Therefore, after complexation with HCNTs, the specific heat of CoHCF/HCNTs is reduced to 2.17 J g^{-1} K^{-1}. The measurement range was −10 to 70 °C with a ramping rate of 5 °C min^{-1}. The detailed calculation is shown in the ESI,† the conversion efficiency at different μ_{HR} is exhibited in Table S1,† and the summary of performance comparison is shown in Table S2.† Apparently, after being complexed with HCNTs, the specific heat is reduced and the charge and discharge capacity of CoHCF/HCNTs improved compared with that of pure CoHCF, which means that Prussian blue analogues composited with carbon materials could further improve the heat-to-electricity conversion efficiency.

4.   Conclusions

In summary, an electrochemical pouch cell based on CoHCF or CoHCF/HCNTs as the working electrode could convert heat into electricity for low-grade thermal energy harvesting. After complexation with HCNTs, the CoHCF/HCNT system exhibits more than twice the heat-to-electricity conversion efficiency exhibited by pure CoHCF at different energy recovery efficiencies (μ_{HR}). These excellent properties arise due to the fact that the CoHCF/HCNT system has a larger absolute temperature coefficient and lower specific heat. All these results provide a new approach to further improve the heat-to-electricity conversion efficiency of TRECs.

Conflicts of interest

There are no conflicts to declare.

Acknowledgements

References

1 I. Gur, K. Sawyer and R. Prasher, *Science*, 2012, **335**, 1454–1455.

2 A. S. Rattner and S. Garimella, *Energy*, 2011, **36**, 6172–6183.

3 M. Zebarjadi, K. Esfarjani, M. Dresselhaus, Z. Ren and G. Chen, *Energy Environ. Sci.*, 2012, **5**, 5147–5162.

4 S. Chu and A. Majumdar, *Nature*, 2012, **488**, 294.

5 B. Poudel, Q. Hao, Y. Ma, Y. Lan, A. Minnich, B. Yu, X. Yan, D. Wang, A. Muto and D. Vashaee, *Science*, 2008, **320**, 634–638.

6 B. F. Tchanche, G. Lambrinos, A. Frangoudakis and G. Papadakis, *Renewable Sustainable Energy Rev.*, 2011, **15**, 3963–3979.

7 G. J. Snyder and E. S. Toberer, in *Materials for Sustainable Energy: A Collection of Peer-Reviewed Research and Review Articles from Nature Publishing Group*, World Scientific, 2011, pp. 101–110.

8 V. I. Birss and C. K. Smith, *Electrochim. Acta*, 1987, **32**, 259–268.

9 Y. Yang, J. Loomis, H. Ghasemi, S. W. Lee, Y. J. Wang, Y. Cui and G. Chen, *Nano Lett.*, 2014, **14**, 6578–6583.

10 C. Crouthamel and H. L. Recht, *Regenerative EMF Cells*, American Chemical Society, 1967.

11 T. Licht and N. Swendeman, *J. Electrochem. Soc.*, 1959, **106**, 616–625.

12 L. B. Anderson, S. A. Greenberg and G. B. Adams, Thermally and Photochemically Regenerative Electrochemical Systems, *Regenerative EMF Cells*, American Chemical Society, 1967, pp. 213–276.

13 M. Rahimi, A. P. Straub, F. Zhang, X. Zhu, M. Elimelech, C. A. Gorski and B. E. Logan, *Energy Environ. Sci.*, 2018, **11**, 276–285.

14 Y. Kuzminskii, V. Zasukha and G. Kuzminskaya, *J. Power Sources*, 1994, **52**, 231–242.

15 Y. Lu, L. Wang, J. Cheng and J. B. Goodenough, *Chem. Commun.*, 2012, **48**, 6544–6546.

16 Y. Yang, S. W. Lee, H. Ghasemi, J. Loomis, X. Li, D. Kraemer, G. Zheng, Y. Cui and G. Chen, *Proc. Natl. Acad. Sci. U. S. A.*, 2014, **111**, 17011–17016.

17 C. Gao, Y. Yin, L. Zheng, Y. Liu, S. Sim, Y. He, C. Zhu, Z. Liu, H. W. Lee and Q. Yuan, *Adv. Funct. Mater.*, 2018, **28**, 1803129.

18 S. W. Lee, Y. Yang, H.-W. Lee, H. Ghasemi, D. Kraemer, G. Chen and Y. Cui, *Nat. Commun.*, 2014, **5**, 3942.

19 Q. Zeng, H. Tian, J. Jiang, X. Ji, D. Gao and C. Wang, *RSC Adv.*, 2017, **7**, 7375–7381.

20 C. Wang, H. Tian, J. Jiang, T. Zhou, Q. Zeng, X. He, P. Huang and Y. Yao, *ACS Appl. Mater. Interfaces*, 2017, **9**, 26038–26044.

21 B. An, S. Xu, L. Li, J. Tao, F. Huang and X. Geng, *J. Mater. Chem. A*, 2013, **1**, 7222–7228.

22 Y. Xia, W.-S. Xiong, Y. Jiang, W. Sun, H.-Q. Sang, R.-X. He, Q. Tai, B. Chen, Y. Liu and X.-Z. Zhao, *RSC Adv.*, 2017, **7**, 21988–21996.

23 S. Qiu, G. Lu, J. Liu, H. Lyu, C. Hu, B. Li, X. Yan, J. Guo and Z. Guo, *RSC Adv.*, 2015, **5**, 87286–87294.

24 X. Zhou, A. Wang, Y. Pan, C. Yu, Y. Zou, Y. Zhou, Q. Chen and S. Wu, *J. Mater. Chem. A*, 2015, **3**, 13011–13015.

25 Y. Zeng, L. Chen, R. Chen, Y. Wang, C. Xie, L. Tao, L. Huang and S. Wang, *J. Mater. Chem. A*, 2018, **6**, 24311–24316.

26 D. Yan, C.-L. Dong, Y.-C. Huang, Y. Zou, C. Xie, Y. Wang, Y. Zhang, D. Liu, S. Shen and S. Wang, *J. Mater. Chem. A*, 2018, **6**, 805–810.

This journal is © The Royal Society of Chemistry 2019

J. Mater. Chem. A, 2019, **7**, 23862–23867 | **23867**